Pre-equilibrium γ-ray emission induced in the ^{40}Ca + ^{48}Ca system at 10 MeV/nucleon and isospin equilibration processes

Massimo Papa,[1,*] Wendong Tian,[4] Gianluca Giuliani,[3] Francesca Amorini,[2,3] Giuseppe Cardella,[1] Alessia Di Pietro,[2] Pier Paolo Figuera,[2,3] Gaetano Lanzalone,[2,3] Sara Pirrone,[1] Francesca Rizzo,[2,3] and Domenico Santonocito[2]

[1]*Istituto Nazionale Fisica Nucleare-Sezione di Catania, Via Santa Sofia 64, I-95123 catania, Italy*

[2]*Istituto Nazionale Fisica Nucleare-Laboratori Nazionali del Sud, Via Santa Sofia 44, I-95123 Catania, Italy*

[3]*Dipartimento di Fisica e Astronomia, Universitá di Catania, Viale Adrea Doria 6, I-95123 Catania, Italy*

[4]*Institute of Applied Physics, CAS, 201800 Shanghai, China*

(Received 3 January 2005; revised manuscript received 30 August 2005; published 15 December 2005)

In the present paper we have studied γ-ray emission in coincidence with charged particles measured in binary processes for the collisions ^{40}Ca + ^{48}Ca, ^{46}Ti at 10 MeV/nucleon. The comparison between γ-ray yields, obtained under identical conditions on the charged particles detected in coincidence, shows an extra yield of around 15 MeV for the ^{40}Ca + ^{48}Ca collision. The analysis of the γ-charged fragment coincidence events, along with the study performed with the dynamical model CoMD-II, explains this effect as the result of a giant dipole resonance emission from the intermediate system, characterized by a high degree of coherence. The performed study aims to establish a link among pre-equilibrium γ-ray emission, initial charge/mass ratio memory effects in the intermediate system for the ^{40}Ca + ^{48}Ca system at short time, and the achievement of a substantial charge/mass ratio or isospin equilibration of the primary fragments formed at longer time. Moreover, the presence of a remarkable extra yield in a restricted range of the γ-ray spectra suggests that this equilibration process evolves through a quasiresonant mechanism.

DOI: 10.1103/PhysRevC.72.064608 PACS number(s): 24.10.−i, 24.60.−k, 24.30.Cz, 21.30.Fe

I. INTRODUCTION

In the past few decades considerable experimental evidence has been collected on giant dipole resonance (GDR) γ-ray emission induced by heavy-ion collisions [1–27]. Pre-equilibrium effects were found at low energy in fusion reactions [6,11,24] and in binary processes for different systems [9,10,13,14,21–23].

The GDR emission in ^{40}Ca + ^{48}Ca and ^{40}Ca + ^{46}Ti systems was studied with particular interest [20–22,25]. These systems have in fact a quite large difference in the charge to mass ratio in the entrance channel whereas the difference in the total mass and mass asymmetry is only 2%. At 25 MeV/nucleon GDR dynamical pre-equilibrium emission was observed in incomplete fusion and binary dissipative reactions by using the γ-ray-particle coincidence method. In those works the pre-equilibrium extra yield was studied by comparing the γ-ray spectra for the two systems extracted with the same conditions on the charged particle coincidence. From the analysis performed on the data at 25 MeV/nucleon, a centroid for the extra yield at about 10 MeV was found in incomplete fusion processes. This evidences a high degree of deformation of the intermediate system. The width of about 6 MeV is related to a characteristic relaxation time τ of about 35 fm/c. Moreover, in Ref. [22], the intensity of the dynamical pre-equilibrium yield with respect to the contribution arising from the statistical mechanism was related to a finite degree of coherence φ_{ch} of the dipolar mode. This parameter evidences memory effects of the difference in the charge/mass ratio between projectile and target. Therefore, study of the evolution of the γ-ray pre-equilibrium effect as a function of bombarding energy, and of the related parameters, appears to assume a wider interest than the one strictly related to the properties of collective motion.

In this work, to characterize the degree of charge/mass asymmetry of a binary system, we will use in the calculations the following parameter [13,14]:

$$R_{NZ} = \frac{1}{2}\frac{A_a A_b}{A_a + A_b}\left[\frac{(N_a - Z_a)}{A_a} - \frac{(N_b - Z_b)}{A_b}\right]. \quad (1)$$

where N, Z, and A are the neutron, proton, and mass numbers of the two partners a and b, respectively. R_{NZ} determines the initial amplitude of the dipolar signal for a binary system resulting from the partition of the total mass and charge between the two partners [14]. This is clearly related to the so-called isospin asymmetry differences of the two nuclei.

In the present work we show the results of the ^{40}Ca + ^{48}Ca ($R_{NZ} = 1.81$) and ^{40}Ca + ^{46}Ti systems ($R_{NZ} = 0.46$) at 10 MeV/nucleon when binary dissipative processes are selected. In particular, in Sec. II we will briefly describe the experimental apparatus. In Sec. III, the experimental results and the criteria adopted for the data analysis will be illustrated. In Sec. IV we will describe the collected experimental results by means of the constrained molecular dynamics model CoMD-II [28] coupled with CASCADE calculations [29]. The CoMD-II model, which is the new version of the CoMD model [30], unlike other semi-classical microscopic models, conserves the total angular momentum. Finally, in the same section we will try to link the memory effects of the entrance channel and the GDR pre-equilibrium emission with the charge/mass or isospin equilibration phenomenon.

*E-mail: papa@ct.infn.it

II. THE EXPERIMENT

The experiment was performed at the Superconducting Cyclotron of the Laboratori Nazionali del Sud (LNS), Catania, Italy. We used two ^{40}Ca beams with energy 9.5 MeV/nucleon and 10 MeV/nucleon impinging on 3 mg/cm^2 and 2 mg/cm^2 thick targets of ^{48}Ca and ^{46}Ti, respectively. Both targets were 95% isotopically enriched. To avoid oxidation, we mounted the targets under a controlled atmosphere. We used the 63 BaF_2 crystals of the multidetector TRASMA described in Ref. [31]. The BaF_2 was placed in a cluster configurations (seven crystals for each cluster) around 45°, 90°, and 135°. They were calibrated during the experiment by using low-energy γ rays emitted by ^{241}Am-^{9}Be, ^{60}Co, and ^{89}Y sources. The reliability of our energy calibration method around the GDR energy was checked by comparing GEANT simulations with cosmic rays and with the 15.1-MeV γ rays from the $p + {}^{12}$C reaction [25,32]. We performed the neutron subtraction using both time-of-flight and pulse shape information from the BaF_2 detectors. Phototube gains were monitered by repeating the calibration procedure several times during the experiment. Moreover, a light signal generated from a light-emitting diode was sent periodically through optical fibers to all crystals during the measurements. These signals allowed a check of the gain stability up to a level of about ±4% during off-line analysis.

Charged fragments in coincidence with γ rays were detected by 24 units of monolithic silicon telescopes. Each of these telescope is a device having five independent ΔE strips (3×4 mm^2) implanted in a common residual energy stage. The first and second stages are 1 μm and 500 μm thick respectively. Two such units mounted on a common ceramic package form a single detection module. The 12 modules used in the experiment were placed 5 cm away from the targets in a symmetric configuration around the beam and covering the polar angular range $\theta = 13°$–$47°$ and an azimuthal angle range in steps of 45°. Details on the monolithic telescopes used can be found in Refs. [33,34]. The good performance of the monolithic detectors allowed us to identify ions up to a charge $Z = 25$ with energy thresholds around 1 MeV/nucleon. As an example we show in Fig. 1 the ΔE-E scatter plot for the detector placed at $\theta_{\rm lab} = 30°$ collected during the measurement of the ^{40}Ca + ^{48}Ca system.

We finally note that with our particle detectors we can measure the charge Z of the detected particles. To get the velocity and kinematical information, to better characterize the studied processes, we assume the fragment mass A of the detected particle equal to the mass of the stable isotope having charge Z.

III. RESULTS

A. Selection of binary reactions

In this section we present the results obtained for the coherent pre-equilibrium γ-ray emission produced in binary processes. These processes are dominant in the angular region covered by our particle multidetector. Therefore, before showing the results from the γ-ray spectra detected in coincidence with particles, we describe the criteria adopted to select the fragment channels. A main point of this measurement is that the geometrical symmetry and the angular range covered by the particle detector system allows, detection, in about 10% of the collected events, multiple coincidence in which at least two γ rays and two particles are detected. These events correspond mainly to the detection of the two reaction partners in kinematical coincidence. This is shown as an example in Fig. 2. In this figure we display a contour plot

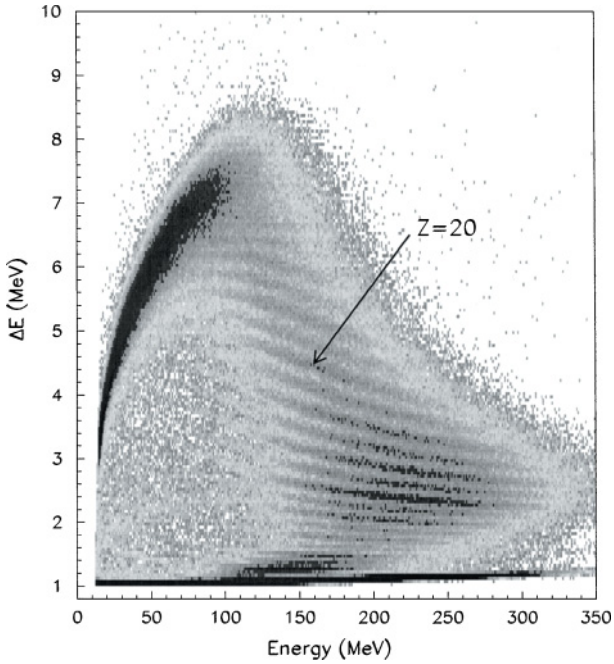

FIG. 1. (Color online) ΔE-E scatter plot related to a monolithic telescope placed at the laboratory angle $\theta_{\rm lab} = 30°$ for the ^{40}Ca + ^{48}Ca reaction at 10 MeV/nucleon incident energies.

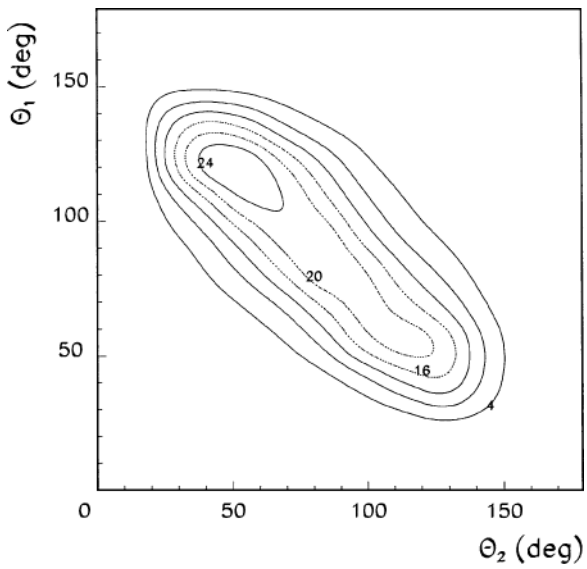

FIG. 2. Contour plot showing, for binary events selected in the ^{40}Ca + ^{46}Ti collision, the center-of-mass angle Θ_1 of the heaviest fragment as a function of Θ_2 related to the second heaviest fragment.

in which the center-of-mass (c.m.) angle Θ_1 of the heaviest fragment is given as a function of the angle Θ_2 for the second fragment. The c.m. angles are computed from the laboratory detection angle, the kinetic energy, and the fragment mass A by applying two-body kinematics relationships. In particular, Fig. 2 refers to the $^{40}\mathrm{Ca} + {}^{46}\mathrm{Ti}$ system and both fragment charges are selected within the interval $Z = 14$–22. This corresponds to the range of fragment charges selected for our final analysis on γ-ray emission, as explained in the following. From the figure it is clearly seen, on average, the typical correlation valid for two-body processes: $\Theta_1 + \Theta_2 \simeq 180^\circ$. Deviations from this behavior are mainly due to secondary evaporation processes that produce a distribution around the average values. Also visible in the figure is a slight anisotropy, corresponding to a light fragment focused around $\Theta_2 \simeq 50^\circ$ and a heavier fragment focused around $\Theta_1 \simeq 130^\circ$. This anisotropy could be related to a relatively fast asymmetric charge splitting inside the selected Z range with a preferential mass transfer from the projectile to the target. In contrast, a more symmetric-charge binary splitting, for which the charge of both fragments lies inside a narrower interval $Z = 16$–22, gives an almost isotropic contribution. This evidence suggests also the presence of a slower symmetric breakup mechanism of the hot compound. The statistics collected for these multiple coincidence events are enough to characterize the binary processes but in sufficient for the study of γ-ray spectra properties in the GDR region. Therefore our analysis of γ-ray pre-equilibrium emission is performed on the much more frequent events produced by the γ-one-particle coincidences. They are selected by finding a set of conditions through an iterative procedure. The charge interval and the upper thresholds on kinetic energies of the fragments are selected in such a way that the spectra of different quantities (charge distributions, c.m. angle distribution, etc.) obtained from the binary coincidence events show behaviors very similar to the spectra corresponding to the γ-one-particle events. The results of this procedure are the following: The charge of the selected fragments varies within the interval $Z = 14$–22, and the laboratory kinetic energy T_{lab} is at most 160 MeV.

Under this condition we can use the γ-one-particle events to study the GDR properties and the related γ-two-particles events to better characterize the binary breakup of the intermediate system. In other words, in this way, on average, we select a region of phase space for which the binary coincidence events represent a restricted sample of events (owing to the limited geometrical efficiency of the multidetector) that are generated essentially by the same reaction mechanism that produces the γ-one-particle selected events.

In Fig. 3 we show an example of comparison between the selected experimental γ-one-fragment and the γ-two-fragments spectra for the $^{40}\mathrm{Ca} + {}^{46}\mathrm{Ti}$ system. In particular, in Figs. 3(a) and 3(d), we show the c.m. angular distribution of the detected fragments computed with the same conditions used to produce the contour-plot shown in Fig. 2. In Figs. 3(b) and 3(e), we show the $\beta_{\mathrm{lab}} = v_{\mathrm{lab}}/c$ spectra in the laboratory reference system. Finally, in Figs. 3(c) and 3(f), we compare the charge distributions in the two cases. The quite similar behavior of the two ensembles of spectra is evident.

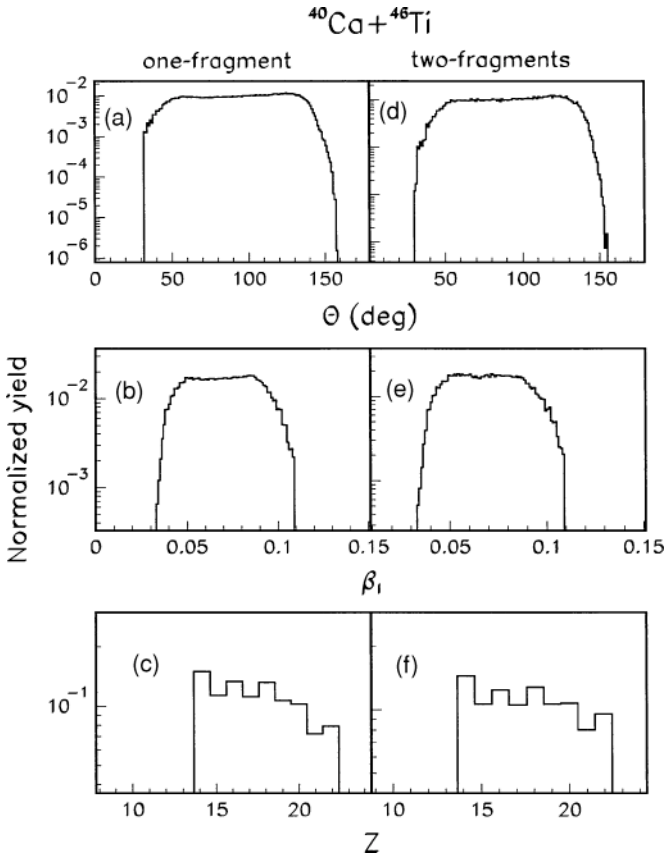

FIG. 3. Mono-dimensional spectra of different quantities for the $^{40}\mathrm{Ca} + {}^{46}\mathrm{Ti}$ colliding system. They have been obtained by analyzing one-fragment and two-fragment events under the selected conditions (see text). For panels (a), (b), and (c) these quantities are obtained for one-fragment events: (a) fragment c.m. angular distribution (b) β_{lab} distribution in the laboratory system, and (c) charge distribution. In panels (d), (e), and (f) the same quantities are plotted as obtained by integrating the two-fragment events; both fragments satisfy the imposed conditions.

In Fig. 4 we show the same spectra displayed in Fig. 3, but for the $^{40}\mathrm{Ca} + {}^{48}\mathrm{Ca}$ system. The comparison between the two figures shows that the selected processes for the two systems are quite similar.

To evidence two-fragment correlations, which are hidden in the one-fragment data, we show on the left panel of Fig. 5, for the selected conditions ($14 \leqslant Z \leqslant 22$ and laboratory kinetic energy $T_{lab} \leqslant 160$ MeV for at least one fragment), the scatter plot of the heaviest fragment having charge Z_{b1} as a function of the lighter one Z_{b2}. More than 90% of the selected events correspond to the quasisymmetric breakup of the system with more than 70% of the total charge detected. The rare events corresponding to a smaller fraction of the total charge do not show correlation in the Z_{b1}-Z_{b2} plane. They are probably due to nonbinary events. In the right panels we show the total kinetic energy loss (T_{KEL}) spectra for the selected γ-two-fragment events computed using the measured kinetic energy of the two detected fragments. In the same panels, we also show the estimated "primary" T_{KEL} spectra (displayed with star symbols) calculated by using a recursive

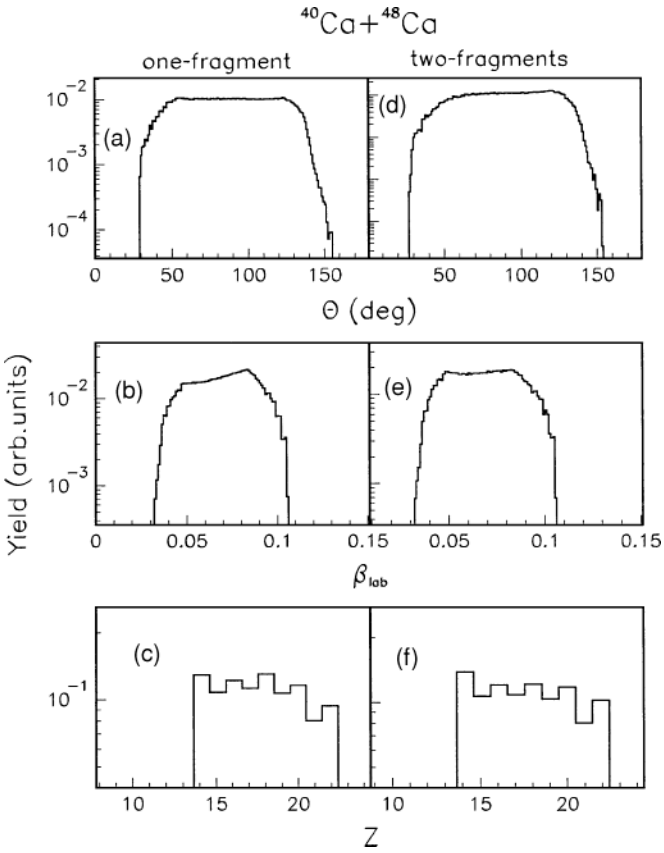

FIG. 4. The same as Fig. 3 but for the ^{40}Ca + ^{48}Ca colliding system.

procedure in which the measured fragment velocities are corrected according to the method suggested in Ref. [35]. This method is based on conservation of total mass and total momentum. The two spectra are quite similar for the system studied. With this method, one can try to estimate the energy loss from secondary evaporation processes and the thick targets used. The reconstructed T_{KEL} spectra using the binary coincidence method show an average value of about 150 MeV.

Knowledge of the mean energy dissipated produced in the primary breakup of the intermediate system enters in the estimation of the statistical GDR emission from the hot fragments. However, this procedure, being based only on general conservation rules, cannot reflect details related to the reaction mechanism. Moreover, it is more suitable for measurement of the involved particle masses, which in our experiment can be only estimated. In Sec. IV, we will try to get a better estimation of the T_{KEL} related to the primary fragmentation by reproducing the observed T_{KEL} spectra using calculations based on the CoMD-II model [28].

B. γ-ray yields

In Fig. 6 we show the γ-ray yields for the two systems studied obtained under the same selected conditions specified in the previous section. The vertical bars represent the uncertainty from the collected statistics. The horizontal bars represent the uncertainty on the γ-ray energy owing to the energy calibration and to the larger binning performed at higher energy to improve the counting statistics. The black lines are statistical model calculations. The parameters have been obtained by a fit procedure that will be discussed in some detail in Sec. IV B. The red line represents the final result, which also takes into account the contribution of dynamical effects, which will be discussed in Secs. IV A and IV C. All calculations have been convoluted with the BaF_2 response functions.

In the inset of same figure we show, as a function of γ-ray energy, the ratio $F = Y^{\mathrm{exp}}_{^{48}\mathrm{Ca}}/Y^{\mathrm{exp}}_{^{46}\mathrm{Ti}}$ between the experimental

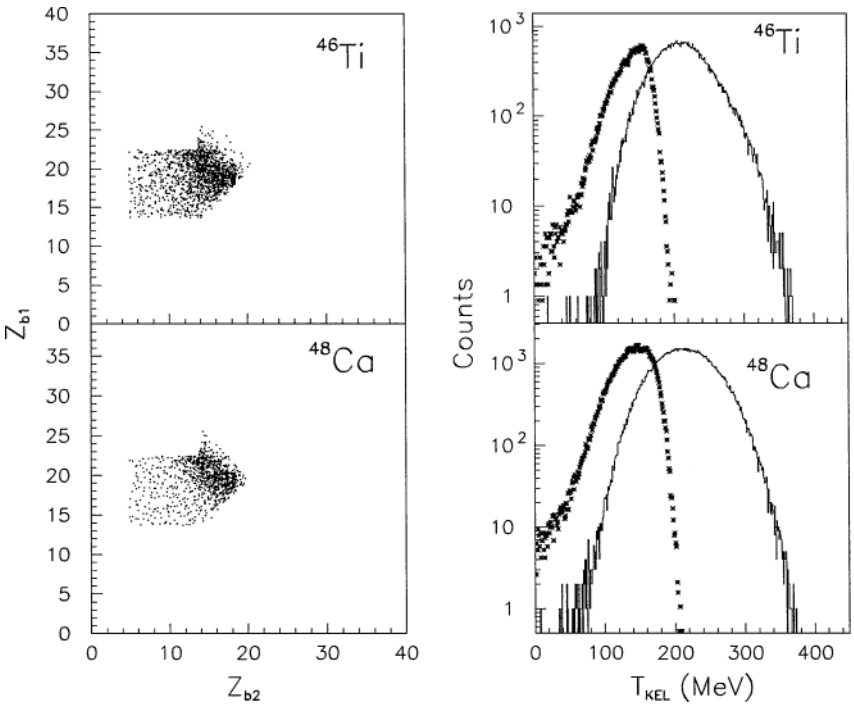

FIG. 5. Left panels: Z_{b1}–Z_{b2} charge scatter plot for binary events in ^{40}Ca + ^{46}Ti (top) and ^{40}Ca + ^{48}Ca (bottom) collisions. At least one fragment satisfies the selected conditions on the charge and threshold energy. Right panels: For the same set of events the T_{KEL} spectra are computed by using measured kinetic energy of the fragments (lines) and applying a recursive procedure to the data, according to the methods suggested in Ref. [35] (star symbols).

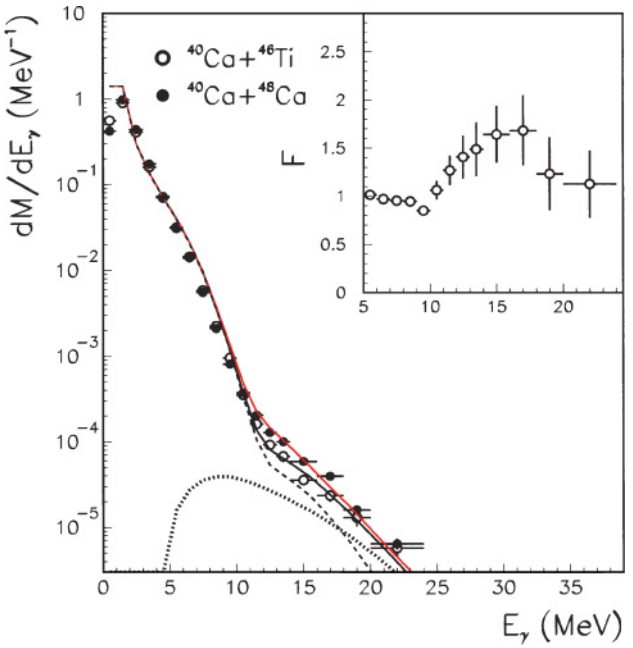

FIG. 6. (Color) γ-ray spectra measured in coincidence with the selected charged fragments for the two colliding systems (symbols). In the inset the ratio F between the γ-ray yield in the ^{40}Ca + ^{48}Ca system with respect to the ^{40}Ca + ^{46}Ti one is also displayed. The black lines display the results of a fit procedure applied to the ^{40}Ca + ^{46}Ti data by means of a statistical model approach (see text). In particular, the dotted line represents the statistical contribution coming from the hot intermediate system, the dashed line is related to the two-fragment contributions (CASCADE calculations), and the full line represents the sum of the previous contributions. The red line represents the sum of the total statistical contribution and the dynamical one. All the calculations have been convoluted with the BaF_2 response functions.

yields obtained for the two systems. The region between 12 and 17 MeV exhibits an extra yield of the system ^{40}Ca + ^{48}Ca when compared to the ^{40}Ca + ^{46}Ti one. Producing such differences, according to the statistical model, requires a 35% increase of the excitation energy (temperature effects) of the compound and of the fragments, or a variation of the produced charge distribution at a level of about 50% [GDR strength factor NZ/A; see Eq. (A1)]. This is not the case for our experimental results, as can be clearly seen by looking at Figs. 3–5. In fact, the behaviors related to different quantities, deduced from the particle analysis, are quite similar for the two systems. This evidence therefore strongly suggests the presence of dynamical effects originated by the only prominent difference characterizing the two systems: the charge/mass ratios in the entrance channels.

IV. DYNAMICAL INTERPRETATION OF THE OBSERVED EXTRA YIELD AND ISOSPIN EQUILIBRATION

A. Main results of dynamical calculations

To describe the dynamical excitation of this pre-equilibrium mode we will use the CoMD-II model [28]. This full N-body approach allows us to treat consistently the fragment formation process and the GDR excitation. In particular, the ensemble average of the dipolar signals generated in many replications, or events, of the same system gives the average dynamical effect. If the average oscillations, triggered by the initial isospin asymmetry, have non-negligible amplitude, a certain degree of coherence or memory between the different replications of the same system exists. In contrast, the collective oscillations out of phase will give rise to the statistical GDR emission [22]. The dynamical calculations were performed using a Skyrme I effective interaction with a compressibility $K = 210$ MeV and an isospin interaction consistent with the liquid-drop mass formula [30]. The nucleon-nucleon hard-core repulsive interaction was simulated by means of free nucleon-nucleon elastic processes with a cross section having a 50-mb upper limit.

The systems ^{40}Ca + ^{48}Ca and ^{40}Ca + ^{46}Ti at 10 MeV/nucleon were studied with the CoMD-II model by generating several thousand events at different impact parameters. The dynamical evolution was followed for a time interval equal of 700 fm/c. After this time, a second stage giving the final particle decay of the excited fragments was simulated using the GEMINI code [36]. We have also applied the main restrictions from the experimental setup (angles and identification energy threshold) and from the selections applied in the experimental data analysis (see previous section). The subset of events obtained in this way can now be compared with the experimental data. In particular, we will perform on these events the ensemble average of the dipolar signals and of the other useful quantities for a description of the main selected process.

As an example of this type of analysis we show in Fig. 7(a), for the ^{40}Ca + ^{48}Ca system, the impact parameter b window selected with the aforementioned restriction on the generated events. The related probability has been computed according to the following equation: $P(b) = 2b\Delta b N(b)/b_m^2 N_o(b)$; $N_o(b)$ and $N(b)$ represent the number of events simulated and the ones selected for a given impact parameter b, respectively; b_m and $\Delta b>$ are equal to 8.4 fm (the sum of the nuclear radii) and 0.25 fm (the step for b), respectively.

In Fig. 7(b) we show, for the ^{40}Ca + ^{48}Ca system, the calculated T_{KEL} spectrum of the primary fragments (dotted line) and the one obtained including secondary evaporation of the excited fragments and the energy loss in the thick target (continuous line). The calculated T_{KEL} spectra were normalized to the corresponding experimental one (shown with closed circles) and smoothed with a continuous function to simplify the comparison. Owing to the finite number of simulated events, the errors on the estimated width and centroid are of the order of 2–3%. In the same figure we show the experimental T_{KEL} spectrum for ^{40}Ca + ^{46}Ti. The calculated T_{KEL} spectrum is quite similar to the experimental ones. The theoretical T_{KEL} related to the primary fragments gives an average value of about 130 MeV. This is about 20 MeV lower than the value estimated by using the procedure of Ref. [35]. This difference can be mostly due to our approximated mass fragment assignment in applying the phenomenological method.

In Fig. 7(c), we show, as an example, the average first time derivative $\overline{V_Z}$, along the Z direction, of the dipolar signals as

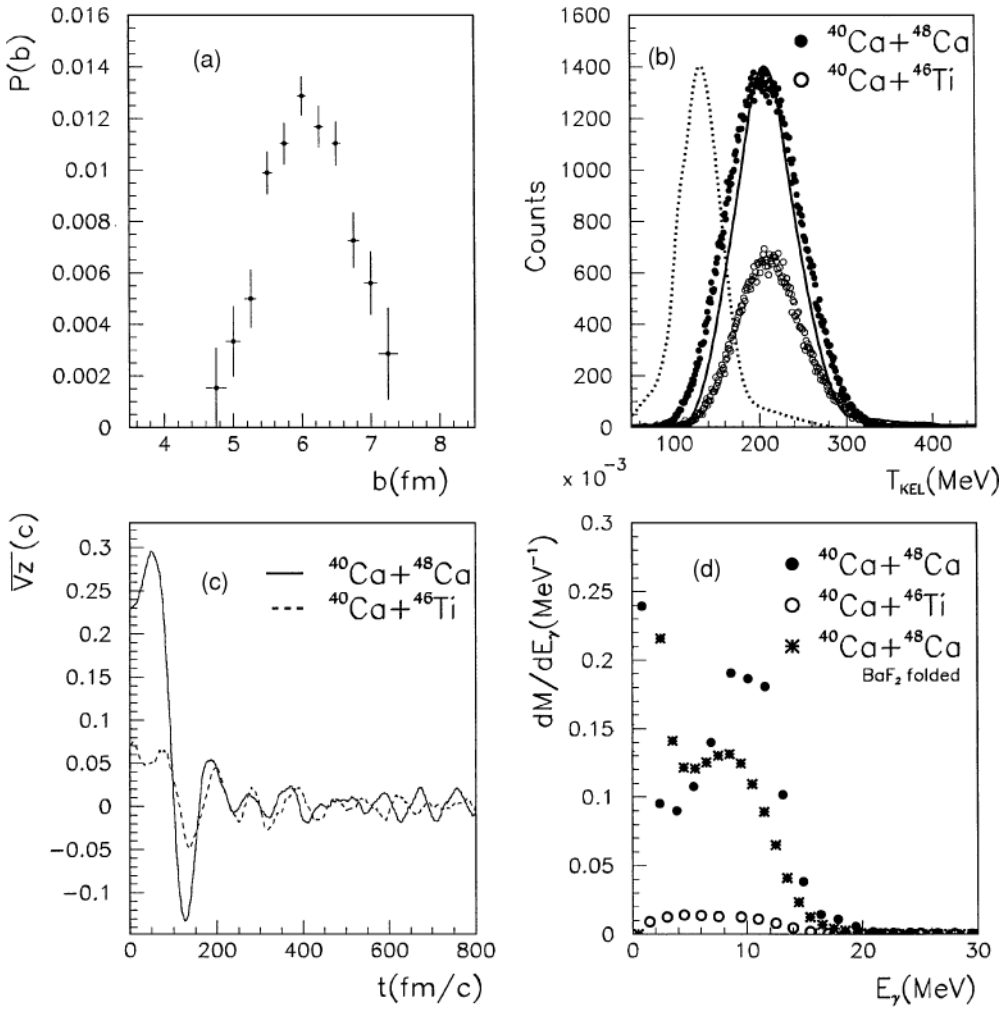

FIG. 7. CoMD II results: (a) impact parameter b window $P(b)$ determined by imposing the same selection conditions applied to the experimental data for the ^{40}Ca + ^{48}Ca system, with error bars related to number of selected events; (b) T_{KEL} of the primary fragements (dotted line) and the one obtained by considering the corrections coming from second-stage evaporation processes and from energy loss in the target (continuous line). It is compared with the experimental data (symbols) for the two investigated systems; (c) average first time derivative $\overline{V_Z(t)}$ of the total dipole along the beam direction evaluated for $b = 6$ fm for the two systems investigated; (d) calculated γ-ray spectra related to the dynamical pre-equilibrium effect.

a function of time for $b = 6$ fm (center of the b window) for the two systems investigated. As can be seen from the figure complete damping of the average oscillation develops in a time interval of about 180 fm/c. In the same time interval also notice the weakness of the dipolar signal for ^{40}Ca + ^{46}Ti compared to the one related to the more charge/mass asymmetric ^{40}Ca + ^{48}Ca system.

The mean lifetime of the intermediate system, changes from about 400 fm/c at around $b = 6$ fm to 200 fm/c at $b =$ 6.75 fm. Therefore we mainly select processes for which the GDR of the intermediate system is out of equilibrium for at least 40% of its lifetime.

For the two systems studied in Fig. 7(d) we show the γ-ray yields related to dynamical effects for all the impact parameters contributing to the process, including the yields produced by the modes along all directions. They have been estimated through the Fourier transform of the second time derivative of the average dipole [14,21,22,37]. Because of the finite time interval of calculation $\Delta t = 800$ fm/c, and according to the properties of the Fourier transform, the energy step is determined according to the following relation: $\Delta E = 2\pi\hbar c/\Delta t$. We note that the maximum of the extrayield is around 10 MeV (circles), whereas the maximum in the measured ratio F is located in the region 12–17 MeV. Some comments on this point will be given in Sec. IV C. The errors on the dynamical estimated yield, which result from the finite number of events on which the average is computed, is of the order of 2%. The calculations for the ^{40}Ca + ^{46}Ti system produce the same scenario for the fragment production; however, the smaller amplitude of the dipolar signal produces a γ-ray yield that is about a factor of 20 weaker at 10 MeV, as can be seen from Fig. 7(d). Finally, with crossed symbols, we show the results obtained for the dynamical yield Y_D^f folded with the BaF_2 response function. Narrow energy steps are necessary

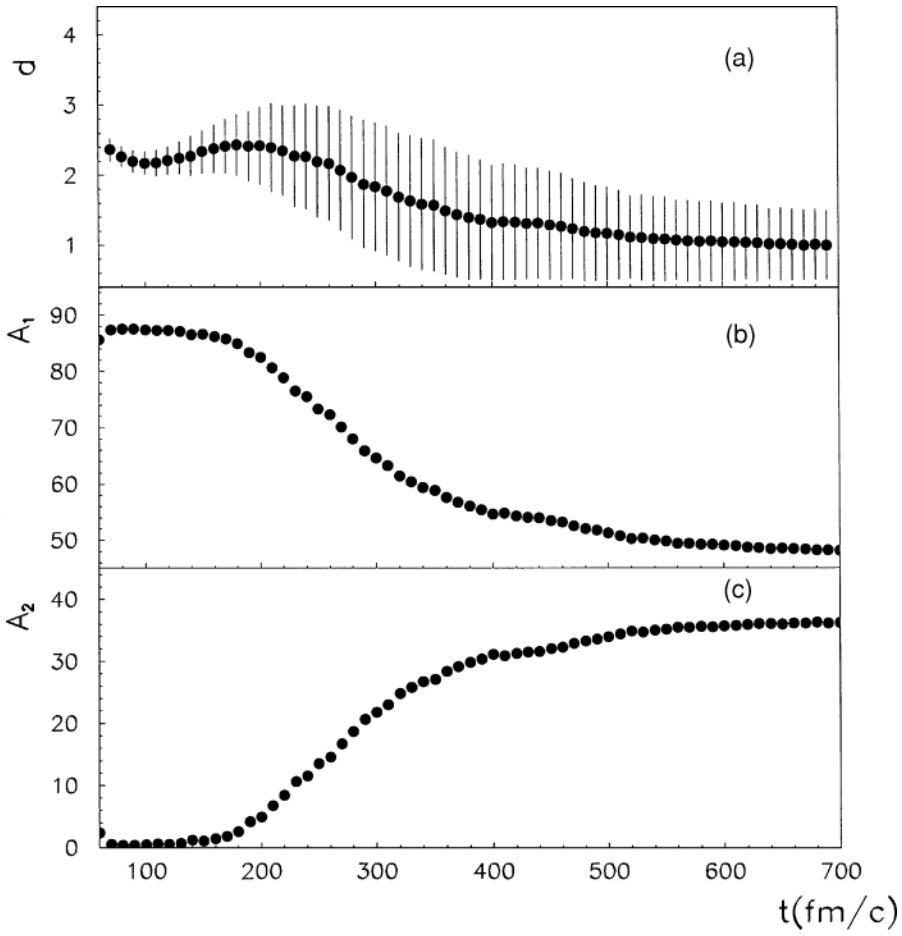

FIG. 8. CoMD-II results for the time evolution of some quantities related to the intermediate system formed in the collision ^{40}Ca + ^{48}Ca at 10 MeV/nucleon and $b = 6$ fm: (a) average ratio d between major and minor axis, with bars indicating the fluctuations around the mean values; (b) average mass of the biggest fragment A_1; (c) average mass of the second biggest fragment A_2.

for comparison with the experimental spectra (see Fig. 6). Therefore the distribution has been obtained by interpolating the theoretical yield calculated from the Fourier transform of the dipolar signals.

Both the experimental studies performed on the binary coincidence events and the CoMD-II calculations allow a description of the main features of the intermediate system breakup for the selected processes. As an example (see also Fig. 8), for the ^{40}Ca + ^{48}Ca system and $b = 6$ fm, the calculations give the following average mass-charge splitting: $A_1 \simeq 47$, $Z_1 \simeq 21$ and $A_2 \simeq 37$, $Z_2 \simeq 17$ around 700 fm/c. Some units of mass and charge can be emitted in the following stage as described with the GEMINI code. By including this small correction, the predicted average charge splitting is in substantial agreement with the experimental one (see also the left panels in Fig. 5).

In particular the R_{NZ} value deduced from the average primary charge/mass break up is about 0.2. This is a rather small value compared with the initial one, $R_{NZ} = 1.81$. Also, at larger impact parameter $b = 6.75$ fm (upper half-width of the selected b window), the final value of R_{NZ} is considerably reduced to about 0.4. This means that, in the selected binary processes, after the breakup of the intermediate system, the isospin degree of freedom evaluated through the model, on average, is almost equilibrated. The equilibration phenomenon or loss of memory is, however, responsible for the dipolar coherent pre-equilibrium γ-ray emission.

B. Dynamical calculations and GDR statistical emission

As shown in the previous sections, the average pre-equilibrium dipolar signal produced in the ^{40}Ca + ^{46}Ti system is quite weak. For this system the γ-ray emission is produced essentially through the statistical mechanism and it could represent the background statistical emission produced in the ^{40}Ca + ^{48}Ca system. Therefore, to estimate the statistical GDR decay coming from the intermediate system in the ^{40}Ca + ^{48}Ca collision and to compare it with the pre-equilibrium yields related to the average dynamics, we have to study in some detail the statistical emission from the ^{40}Ca + ^{46}Ti system. In particular, we have to estimate the contribution coming from the intermediate system and the one produced by the fragments.

The dynamical calculations presented in the previous section are in substantial agreement with the data from the two-fragment coincidence measurement. Therefore they allow, with a good confidence level, a trace back in time of the evolution of the studied system. In particular, they allow us to identify and characterize, apart from the dynamical pre-equilibrium γ-ray emission, the sources that contribute to the GDR statistical γ-yield. For example, for the system ^{40}Ca + ^{46}Ti at $b = 6$ fm, the intermediate system survives up to an average time of about 400 fm/c. Moreover, it produces two excited fragments with an average excitation energy of about 1.3 MeV/nucleon and mass and charge partitions that are, within 10%, similar to the ones related to the ^{40}Ca + ^{48}Ca

system. About 15% of the calculated $T_{\rm KEL}$ is due to particle emission of the hot source before it breaks up into two fragments. Therefore we will use the CoMD-II calculations as a reference starting point or a guideline to reproduce, within the framework of the statistical model, the γ-ray contribution produced from the ^{40}Ca + ^{46}Ti system.

The results of the statistical model calculation are shown in Fig. 6 together with the experimental data. The calculations have been convoluted with the BaF_2 response functions. To estimate the contribution produced by the two fragments (dashed line in Fig. 6) we used information from microscopic calculations of excitation energies, masses, charge, and total angular momentum. The GDR damping widths have been chosen according to the study of systems ranging from $A = 45$ to $A = 208$ performed in Ref. [15]. In that work, based on Landau theory applied to hot rotating nuclei, a simple phenomenological function $\Gamma(A, T, J)$ (see Eq. (4) of the Ref. [15]) describes reasonably well the experimental data collected in this range of masses.

The GDR energy centroids for different masses have been calculated according to the relation $E_{\rm GDR} = 31.2A^{-\frac{1}{3}} + 20.6A^{-\frac{1}{6}}$. The values for these parameters have been used as input values for CASCADE calculations [29]. As an example, for a fragment of mass $A = 45$, total excitation energy 1.3 MeV/nucleon ($T \simeq 3$ MeV), and total spin $15\hbar$, we get a Γ value of about 12 MeV. The final result has been obviously obtained by summing over all the contributing impact parameters according to the b window determined from dynamical calculations.

The contribution from the hot intermediate stage (excitation energy about 2.3 MeV/nucleon, $T \simeq 4$ MeV) is strongly affected by the dynamics leading to the binary breakup. It is in fact quite localized in time and a pre-equilibrium light-particle emission is present, contributing 15% to $T_{\rm KEL}$. Moreover, the intermediate system is strongly deformed with a prolate shape. The average ratio d between the two main axes can reach large values (about 2.4 at around 200 fm/c). Both the average values and the fluctuations around this mean value change in time (see Fig. 8). These clear nonequilibrium features motivate a different choice in the description of the statistical γ-ray yield coming from this stage. As shown in Ref. [22] the statistical contribution could be evaluated by means of a fully dynamical approach in which the spectral properties of the fluctuations on the dipolar signal are analyzed. In the present work, we will try to describe this contribution in a simpler phenomenological way. The yield has been in fact described by supposing the decay of a hot deformed and rotating source (with an average total spin equal to about $50\hbar$) modeled through a modified sum $L(E_\gamma, J, T)$ of two Lorentian functions and a thermal exponential factor from the level density expression [14,16]. More details of the functional form of the $L(E_\gamma, J, T)$ factor are given in Appendix A.

The modification made to the $L(E_\gamma, J, T)$ yield is the following:

$$\frac{dM}{dE_\gamma} \equiv L'(E_\gamma, J, T) = K_s \left(\frac{\Gamma_D}{\Gamma_D + \Gamma_{\rm cn}}\right) L(E_\gamma, J, T), \quad (2)$$

where Γ_D represents the width related to the decay time τ_D of the dynamical dipolar mode [5,14,38,39]. This time determines the strength of the coherent emission in the ^{40}Ca + ^{48}Ca system and well approximates the finite time necessary to excite the statistical GDR mode in the same system and in the ^{40}Ca + ^{46}Ti one [14,22]. According to the calculation performed in the present work Γ_D is about 4 MeV [see Fig. 7(d)]. $\Gamma_{\rm cn}$ takes into account the intermediate system lifetime, including the binary decay width as estimated from CoMD-II calculations. Finally, K_s is a correction factor representing the emission from different steps of the cascade before the breakup. We have considered as fit parameters the K_s factor, the energy centroid E_0 of the two Lorentians, and the associated damping width $\Gamma(0, T)$ (see Appendix A). The results of the fit for the ^{40}Ca + ^{46}Ti system are the following: $K_s = 3.2 \pm 0.8$, $E_0 = 16 \pm 1.5$ MeV, and $\Gamma(0, T) = 11.5 \pm 1$ MeV.

The sum of the convoluted contributions of the fragments (dashed line) and the one associated with the intermediate system (dotted line) is plotted in Fig. 6 with a continuous black line. From the figure it is possible to see that, at 12 and 17 MeV, the fraction α of the statistical GDR emission from the intermediate system with respect to the total contribution varies between 0.25 and 0.5. We have also verified that these ratios are essentially preserved even for a variation of the fit parameters within 20%.

C. Comparison between statistical and dynamical γ-ray emission: degree of coherence

In the inset of Fig. 6 we have shown the ratio F between the γ yield produced in the ^{40}Ca + ^{48}Ca collision with respect to that of the ^{40}Ca + ^{46}Ti one. The horizontal bars indicate the uncertainty on the energy owing to the spectra binning. Within the errors a maximum of the average trend, $F \simeq 1.7$, can be identified around 15 MeV. The confidence level on the presence of this maximum is about 80%–90%. This evaluation has been performed by comparing the χ^2 values obtained by fitting the average trend with different types of functions, one class allowing for the presence of a maximum (combinations of Gaussian and exponentials) and another characterized by a monotonic behavior in the studied energy range (second-order polynomials and square-root function). This latter class of functions is able to give, in the best case, a confidence level of about 22%.

The effectiveness of the convoluted pre-equilibrium strength $Y_D^f(E)$, computed with the CoMD-II model [see Fig. 7(d)] to explain the observed overstrength, is evident by looking at Figs. 6 and 9. In Fig. 6 the red line represents the total calculated γ-ray yield estimated by summing the statistical contributions to the dynamical one. The global improvement in the quality of the fit with respect to the case in which only the statistical contribution is taken into account is clearly evident.

In Fig. 9 we instead perform a comparison that is independent of the the calculation based on the CASCADE model but that is still based on the hypothesis that the γ-ray statistical contribution produced from the ^{40}Ca + ^{48}Ca system is well approximated by the ^{40}Ca + ^{46}Ti one. In particular, in this

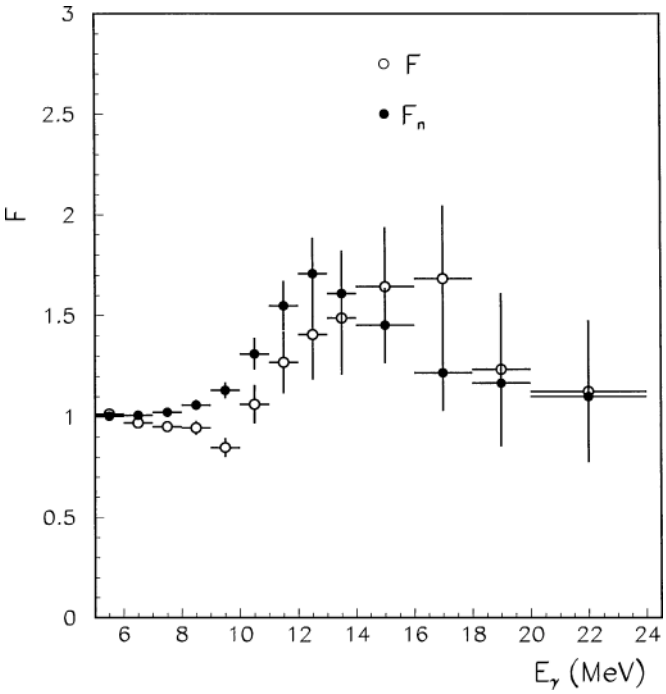

FIG. 9. Ratio F of the γ-ray yield for the two systems studied (already shown in the inset of Fig. 6) as a function of energy (open circles), compared with F_n defined in Eq. (3) (closed circles).

figure we plot, with open circles, the experimental ratio F (already shown in the inset of Fig. 6) and we compare it with the ratio F_n (closed circles) defined through the following relation:

$$F_n \equiv \frac{Y^{\rm exp}_{^{46}\rm Ti}(E) + Y^f_D(E)}{Y^{\rm exp}_{^{46}\rm Ti}(E)}. \quad (3)$$

Figure 9 shows that the obtained values of F_n well approximate the measured F in the range $E_\gamma = 13$–16 MeV, within the uncertainties related to our measurements. In particular even if the maximum of the evaluated dynamical yield Y^f_D is centered at 9 MeV [see Fig. 7(d) and Sec. IV A), the different shapes of the dynamical yield with respect to the statistical one shift the maximum in the ratio F_n to 13 MeV. However, an overestimation at lower energies seems to showup. A dynamical yield centered at higher energy would better reproduce the ratio F. Calculations are in progress to understand whether a fully dynamical evaluation of the γ-ray yield that includes also the statistical contribution from the hot deformed compounds [22] can explain these differences.

We want to conclude this section by characterizing, in a more quantitative way, the behavior of the intermediate systems formed in the $^{40}\rm Ca + ^{48}Ca$ collision with respect to the dipolar γ-ray emission in the GDR region. To this aim, in the study performed in Ref. [22] a degree of coherence $\varphi_{\rm ch}$ of the emitted radiation from the intermediate source was defined as a function of time. In the present work, we want to define a parameter having the same physical meaning but that can be more easily extracted from the experimental data. By assuming that the dynamical yield can be experimentally estimated as $Y^{\rm exp}_D = Y^{\rm exp}_{^{48}\rm Ca} - Y^{\rm exp}_{^{46}\rm Ti}$, we can define the degree of coherence as follows:

$$\Phi_{\rm ch}(E) \equiv \frac{Y^{\rm exp}_D(E)}{Y_{\rm cn}(E) + Y^{\rm exp}_D(E)} = \frac{F(E) - 1}{\alpha(E) + F(E) - 1}, \quad (4)$$

$$F(E) \equiv \frac{Y^{\rm exp}_{^{48}\rm Ca}}{Y^{\rm exp}_{^{46}\rm Ti}}, \quad (5)$$

$$\alpha(E) \equiv \frac{Y_{\rm cn}}{Y^{\rm exp}_{^{46}\rm Ti}}. \quad (6)$$

These definitions are based on average γ-ray multiplicities at different γ-ray energies, rather than the corresponding released energy as in Ref. [22].

The quantity $Y_{\rm cn}$ is the γ-ray yield produced through a statistical mechanism from the hot compound, which we suppose (as a first-order approximation) to be the same for the two systems studied. The evaluation of this quantity (α coefficient) requires a model interpretation of the dynamics in processes leading to fragment production. However, using a high performance experimental apparatus with a good reconstruction power for the emitted sources can provide strong restriction on the model interpretation. The ratio F by definition is a directly measurable quantity. In particular, $\Phi_{\rm ch}(E)$ by definition is 0 if the dynamical contribution is zero; it reaches the maximum value 1 in the extreme situations in which the parameter α is equal to 0.

For the investigated system, according to the performed study, at $E_\gamma = 15$ MeV, we can estimate $\alpha \simeq 0.5$ and $F \simeq 1.7$, and therefore we obtain $\Phi_{\rm ch} = 0.6 \pm 0.2$. (Practically the same value is obtained at 12 MeV.) The system $^{40}\rm Ca + ^{48}Ca$ studied in incomplete fusion reactions at 25 MeV/nucleon [21, 22,25] gives $\alpha \simeq 1$ with $\Phi_{\rm ch} = 0.3 \pm 0.03$ for γ-ray energies around 10 MeV. The difference in the extracted $\Phi_{\rm ch}$ parameters is due essentially to the fact that in the incomplete fusion processes at 25 MeV/nucleon we have the contribution of one source. This hot source will emit down to the end of the cascade. Therefore the statistical emission in this case will have a relevant weight ($\alpha \simeq 1$). In contrast, in the present case the binary selected events also determine the selection of intermediate sources (colder than the 25 MeV/nucleon case), which, after some hundreds of fm/c, decay into two fragments. During this relatively short time interval, the coherent emission plays a prominent role.

D. Pre-equilibrium γ-ray emission and isospin equilibration

The existence of a finite degree of coherence highlights (see also Ref. [22]) the formation of an intermediate system in which the GDR mode is not equilibrated for a time interval comparable to the mean lifetime of the hot sources. During this time, the source is dominated by memory effects of the entrance channel. None the less, the observation of a considerable degree of coherence in the γ-ray emission can be assumed as a typical signal related to a considerable average isospin equilibration of the produced fragments.

This last point can be emphasized by looking at Fig. 10. In Fig. 10(a) we show, for two different cases, the average first time derivative $V_Z(t)$ of the total dipolar signals computed along the major axis of a dinuclear system. This hypothetical

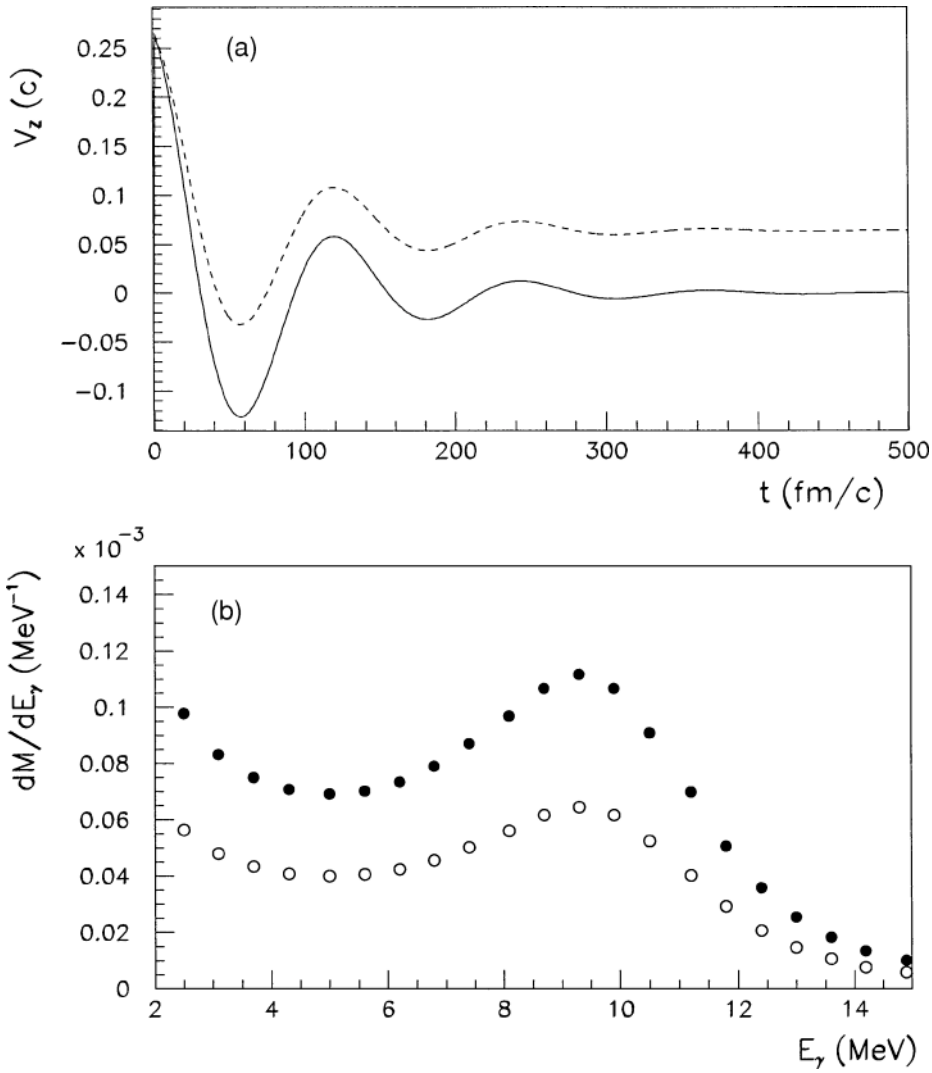

FIG. 10. (a) Average dipolar signals for two possible evolutions of the $^{40}Ca + ^{48}Ca$ system at 10 MeV/nucleon evaluated with a harmonic approximation. The examples shown are referred to two possible time evolutions of V_Z related to a dinuclear system. The dipolar signals have the same mean lifetime (80 fm/c) but correspond to different isospin asymmetries of the final system (see text). Total and partial equilibration of the charge/mass ratio are shown by solid and dashed lines, respectively. (b) Related γ-ray emission probability for total and partial equilibration of the charge/mass ratio are shown by closed circles and open circles, respectively.

system is supposed to have an average lifetime greater than the damping time τ_D of the dipolar oscillations. These one-dimensional calculations are performed for simplicity in the harmonic approximation (see the Appendix in Ref. [22]), neglecting the fluctuations in the charges and masses of the two fragments. However, we note that this schematic example does not allow for a strict comparison with the absolute yield produced through three-dimensional and self-consistent calculations like the CoMD-II ones. Nevertheless, this example can well illustrate the sensitivity of the dynamical yield to the degree of equilibration of the charge/mass ratio that the system can attain.

Both signals have a mean lifetime of $\tau_D = 80$ fm/c and a main frequency corresponding to 10 MeV. The systems have the same initial values $V_Z(0)$ but different final values owing to the different charge/mass or isospin equilibration degree. Therefore we can write [22]

$$V_Z(t \gg \tau_D) = R_{NZ}(t)\frac{dR}{dt}. \tag{7}$$

$\frac{dR}{dt}$ represents the outgoing relative velocity of the two primary fragments, which in this case we suppose to be the same for the two systems. In such a way, apart from the degree of isospin equilibration, the two processes are strictly equivalent. In particular, the full line represents the average dipolar signal of a binary system, which has totally equilibrated the charge/mass ratios [$R_{NZ}(t \gg \tau_D) = 0$; therefore $V_Z(t \gg \tau_D) = 0$]. This case can mimic the result obtained from CoMD-II calculations shown in Fig. 7(c) for $b = 6$ fm. In that case the dipolar signal at long time is on average zero. In the other case, displayed in Fig. 10(a) with a dashed line, the charge/mass ratio-reaches about one-fourth [$R_{NZ}(t \gg \tau_D) = 0.46$] of the initial value. In Fig. 10(b) we show the corresponding pre-equilibrium yield. The partially equilibrated system (open circles) shows a dynamical yield, and therefore a degree of coherence that is about 50% lower than the other one.

We can therefore conclude that the experimental data on γ-ray emission collected for the studied system together with the CoMD-II results strongly support a substantial isospin equilibration of the $^{40}Ca + ^{48}Ca$ system obtained through

dipolar coherent emission [see Fig. 7(c)]. Moreover, the uncertainty of the experimental data on the $1 - F = Y_D^{\rm exp}(E)/Y_{^{46}{\rm Ti}}^{\rm exp}$ value gives, at 14 MeV, a lower limit greater than about 0.3 (the measured value is about 0.7 see the inset in Fig. 6) and therefore the schematic example discussed in this section allows us to estimate an upper limit for the R_{NZ} final value of about 0.5.

In a more general way we want also to note that the observation of a high degree of coherence is related to the rather narrow width of the pre-equilibrium contribution generated from the average oscillations of the dipolar signal. Moreover, the experimental evidence collected so far on this phenomenon shows a degree of coherence that is clearly different from zero in a restricted region of the γ-ray spectrum (from 10 to 15 MeV) with values in most cases larger than 25% [9–11,13,14,22–25]. This means that, at the investigated incident energies (8–25 MeV/nucleon) and within the experimental uncertainties, the equilibration of the charge/mass degree of freedom could evolve through a quasiresonant mechanism for which the damping Γ_D of the dynamical mode is smaller than the related resonance energy E_D ($\pi\Gamma_D \sim E_D$). This mechanism differs from the so-called 'isospin-diffusion' (see, e.g., [40,41]) process observed at higher energies in which, also according to the terminology used, the dipolar average collective motion should be over-damped or $\pi\Gamma_D \gg E_D$. In this last case we could predict a strong reduction of the extra-yield intensity (also up to one order of magnitude around 10–15 MeV) but extending in a larger E_γ energy interval. This mechanism could give rise to the coherent nucleon-nucleon bremsstrahlung effect.

We now consider a generalization of Eq. (7) for realistic processes leading to many particles in the final states and then we include the effect of fluctuations in charges, masses, and momenta of the produced particles. These conditions are typical for higher energies and we obtain the following expressions for the ensemble average of first time derivative of the total dipole $\vec{V}$:

$$\overline{\vec{V}(t\to\infty)} = \sum_{A,Z} \frac{Z}{A} \overline{m_{Z,A}} \overline{\langle\vec{P}\rangle_{Z,A}} C^{Z,A}_{\langle\vec{P}\rangle}, \tag{8}$$

$$C^{Z,A}_{\langle\vec{P}\rangle} = \frac{\overline{m_{Z,A}\langle\vec{P}\rangle_{Z,A}}}{\overline{m_{Z,A}}\,\overline{\langle\vec{P}\rangle_{Z,A}}}, \tag{9}$$

$$\overline{\vec{V}(t\to\infty)} = \overline{\vec{V}(t > t_{\rm eq})}. \tag{10}$$

The bar symbol indicates the ensemble average; $\overline{m_{Z,A}}$ and $\overline{\langle\vec{P}\rangle_{Z,A}}$ represent the average multiplicity and the mean momentum of the produced particles respectively; and $C^{Z,A}_{\langle\vec{P}\rangle}$ is the correlation function between multiplicity and the mean momentum. Therefore $\overline{\vec{V}}$ is directly linked with a kind of weighted average of the charge/mass ratio, which takes into account also the average isospin flow direction via the $\overline{\langle\vec{P}\rangle_{A,Z}}$ factors. This weighted average does not depend directly on the yield of the produced free neutrons. Obviously, the indirect dependence is due to the total momentum conservation rule. Finally, Eq. (10) states that $\overline{\vec{V}}$ is invariant with respect to statistical emission processes, which we can suppose to take place after a time $t_{\rm eq}$. This last feature makes particular attractive the study of this global variable. A simple demonstration of these equations is given in Appendix B for completeness.

All the quantities appearing in Eq. (8) are in principle directly measurable through good charge and mass particle identification and the obtained value of $\overline{\vec{V}}$ can be associated with the primary stage of the process. In real cases, a bias term, evaluated by studying the analogous charge/mass symmetric system, can be subtracted to take into account all the effects related to the incomplete event reconstruction.

We can therefore foresee that the natural evolution of the study performed on the subject treated in the present work should include high- efficiency measurements of the γ-pre-equilibrium emission in coincidence with fragments and particles (identified in charge and mass). The information $[\overline{\vec{V}(t_{\rm eq})}, \Phi_{\rm ch}(E), Y_D^{\rm exp}(E)]$ extracted from these measurements can give a ful understanding of the charge/mass equilibration process including its strength, the mechanism through which it evolves (quasiresonant or overdamped motion), and the characteristic times involved. The related time scale can then be evaluated through the study of the spectral properties of the associated pre-equilibrium γ-ray emission. Obviously, this information could be related to the main ingredients of the nucleon-nucleon effective interaction, in particular the isovectorial one, allowing us to obtain a useful reference point for a better knowledge of the nuclear forces.

V. FINAL REMARKS

In the present work we have discussed the dipolar pre-equilibrium γ-ray emission observed in the $^{40}{\rm Ca} + {}^{48}{\rm Ca}$ system at 10 MeV/nucleon for binary dissipative processes. The pre-equilibrium emission has been studied by comparing this system with the charge/mass quasisymmetric system $^{40}{\rm Ca} + {}^{46}{\rm Ti}$. The binary dissipative processes have been characterized by studying the kinematics coincidence events. The fragment correlations included in the $T_{\rm KEL}$ and in the average charge split of the binary processes have been reproduced by the CoMD-II dynamical calculations. These calculations within the selected b window allow us, with a reasonable confidence level, to extract more information on the primary fragmentation and on the mean lifetime of the intermediate source. The study performed allows the determination of the degree of coherence $\Phi_{\rm ch} \simeq 0.6 \pm 0.2$ of the emitted radiation around E_γ =15 MeV. The obtained degree of coherence is about twice that measured at 25 MeV/nucleon in incomplete fusion processes.

Moreover, calculations based on the CoMD-II model and the illustrated properties of the first time derivative of the total dipole $\overline{\vec{V}}$ allow linking the observed degree of coherence and the intensity of the dynamical emission to the isospin or charge/mass equilibration process. According to the obtained experimental results discussed in this paper and other previous data collected for binary dissipative processes in the energy interval 8–25 MeV/nucleon, [9–11,13,14,22–25], the

observed pre-equilibrium γ-ray emission could be related to a substantial charge/mass equilibration between the two reaction partners. The observation, within the experimental errors, of a strong pre-equilibrium γ-ray emission in a restricted E_γ energy interval suggests a quasiresonant mechanism for the isospin equilibration process at these energies.

ACKNOWLEDGMENTS

We thank Mr. C. Marchetta for his careful handling of the ^{48}Ca target and Dr. E. DeFilippo, Mr. F. Ferrera, andquantity Mr. G. Del Tevere for software assistance. Finally, we thank also Dr. J. Winfield for the kind and careful revision of the text.

APPENDIX A

In this Appendix we recall some details of the formula expressing the GDR γ-ray yield predicted according to the statistical decay of a hot-deformed rotating compound nucleus $L(E_\gamma, J, T)$. This function has been used in Sec. IV B to estimate the yield produced from the decay of the intermediate system formed in the reactions under study. According to compound nucleus theory and to various experimental data collected so far (see, e.g., Ref. [2]), for a prolate ellipsoid, $L(E_\gamma, J, T)$ can be expressed by the following expression:

$$L(E_\gamma, J, T) = \rho_{f,i}(T, J)\frac{4e^2}{\pi\hbar\Gamma_{\rm cn}m_0c^3}\frac{NZ}{A} \times \sum_{j=1}^{2}\frac{S_j\Gamma_j E_\gamma^4}{\left(E_\gamma^2 - E_j^2\right)^2 + (E_\gamma\Gamma_j)^2} \quad \text{(A1)}$$

with $S_1 = 1/3$ (one major axis) and $S_2 = 2/3$. The first factor represents the level density ratio. It contains the main dependence from the temperature and total angular momentum of the compound system. N, Z, and A are the neutrons, protons, and total mass number of the compound system, respectively. The Γ_j and E_j represent the damping width and the GDR energy centroid related to the motion along the principal axes; $\Gamma_{\rm cn}$ is the total width related to the compound lifetime. According to the aforementioned references, these quantities can be expressed through the analog quantities for the spherical system, $E_0, \Gamma(0, T)$, by the following relations:

$$\frac{E_1}{E_2} = 0.91\frac{d_2}{d_1} + 0.089, \quad \text{(A2)}$$

$$E_0 = \tfrac{1}{3}E_1 + \tfrac{2}{3}E_2, \quad \text{(A3)}$$

$$\Gamma_j = \Gamma(0, T)\left(\frac{E_j}{E_0}\right)^\delta, \quad \text{(A4)}$$

$$\delta = 1.6, \quad \text{(A5)}$$

where d_1 and d_2 represent the axis elongations.

In particular, these expressions were determined in a phenomenological way from the GDR ground-states properties. According to Ref. [16], they remain valid at finite temperature.

APPENDIX B

In this Appendix we want to clarify the definition and properties of the ensemble average of the first time derivative of the total dipole $\overline{\vec{V}}$ expressed through Eqs. (8)–(10). This simple derivation can be useful since it naturally produces an explicit definition of the correlation functions introduced in Eq. (9) in terms of an event-by-event analysis performed on the experimental data.

In the following, we will describe the multiparticle event at very long time when all the fragments are cold. In this limit and for our aims, the disassembly of the system can be described through the velocities $\vec{v}_i^k$, the charges Z_i^k, or the mean momentum $\langle\vec{P}_{Z,A}^k\rangle$ and the multiplicity $m_{Z,A}^k$ of the particle i having charge Z and mass A in the generic event k. Therefore, we can write the following set of identities:

$$\vec{V}^k(t\to\infty) = \sum_{i=1}^{M^k} Z_i^k\vec{v}_i^k = \sum_{Z,A}\frac{Z}{A}m_{Z,A}^k\langle\vec{P}\rangle_{Z,A}^k, \quad \text{(B1)}$$

$$\sum_{Z,A} m_{Z,A}^k = M^k, \quad \text{(B2)}$$

$$\langle\vec{P}\rangle_{Z,A}^k = \frac{\sum_{l=1}^{m_{Z,A}^k}\vec{P}_l^k}{m_{Z,A}^k}, \quad \text{(B3)}$$

where the index l varies over all the particles having the same mass A and charge Z in the event k.

By performing the ensemble average on N events, we obtain

$$\overline{\vec{V}(t\to\infty)} = \sum_{Z,A,k=1}^{N}\frac{Z}{A}\frac{m_{Z,A}^k\langle\vec{P}\rangle_{Z,A}^k}{N} = \sum_{Z,A,k=1}^{N}\frac{Z}{A}\overline{m_{Z,A}}\,\overline{\langle\vec{P}\rangle_{Z,A}}\,C_{\langle\vec{P}\rangle}^{Z,A}, \quad \text{(B4)}$$

$$C_{\langle\vec{P}\rangle}^{Z,A} \equiv \frac{\overline{m_{Z,A}\langle\vec{P}\rangle_{Z,A}}}{\overline{m_{Z,A}}\,\overline{\langle\vec{P}\rangle_{Z,A}}} = N\frac{\sum_{k=1}^{N} m_{Z,A}^k\langle\vec{P}\rangle_{Z,A}^k}{\left(\sum_{k=1}^{N} m_{Z,A}^k\right)\left(\sum_{k=1}^{N}\langle\vec{P}\rangle_{Z,A}^k\right)}. \quad \text{(B5)}$$

These equations clarify the meaning of Eqs. (8) and (9).

To prove the validity of Eq. (10) we now consider a shorter time t and we suppose that the produced fragments are now excited. Consequently, the expression of $\vec{V}^k$ for the event k can be written as

$$\vec{V}^k(t) = \sum_{i=1}^{M'^k} Z_i'^k\vec{v}_i'^k + \sum_{i=1}^{m^k}\vec{S}_i. \quad \text{(B6)}$$

The primed symbols represent the different quantities evaluated at time t. $\vec{S}_i$ stands for possible dipolar intrinsic excitations of the complex fragments that are produced with a multiplicity m^k. We can now suppose for simplicity and without losing generality that the chosen time t is such that

$$Z_i'^k = Z_i^k, \quad i = 1, \quad M'^k - 1 \tag{B7}$$

$$\vec{v}_i'^k = \vec{v}_i^k, \quad i = 1, \quad M'^k - 1 \tag{B8}$$

$$M'^k = M^k - 1. \tag{B9}$$

We can also suppose that the last fragment M'^k will subsequently decay into the fragments labeled with indexes $M^k - 1$, and M^k observed at longer time [see Eqs. (B1)–(B3)]. Therefore

$$Z'^k_{M'^k} = Z^k_{M^k-1} + Z^k_{M^k}, \tag{B10}$$

$$\vec{v}^k_{M^k-1} = \vec{v}'^k_{M'^k} + \vec{v}_r^{M^k-1}, \tag{B11}$$

$$\vec{v}^k_{M^k} = \vec{v}'^k_{M'^k} + \vec{v}_r^{M^k}, \tag{B12}$$

$$\vec{V}^k(t \to \infty) = \vec{V}^k(t) + Z^k_{M^k-1}\vec{v}_r^{M^k-1} + Z^k_{M^k}\vec{v}_r^{M^k} + \sum_{i=1}^{m^k} \vec{S}_i, \tag{B13}$$

where $\vec{v}_r^{M^k-1}$ and $\vec{v}_r^{M^k}$ are the relative velocities of the particles $M^k - 1$ and M^k with respect to the common c.m. velocity $v'^k_{M'^k}$. In the following, for simplicity, we perform an ensemble average on all the events having this structure. In other words, we perform an ensemble average on the process leading to the particle decay of the fragment M'^k. The results obtained with this average obviously will remain valid for a more extended average, which includes events having different structures:

$$\overline{\vec{V}^k(t \to \infty)} = \overline{\vec{V}^k(t)} + \overline{Z^k_{M^k-1}}\,\overline{\vec{V}_r^{M^k-1}} C_{M^k-1} + \overline{Z^k_{M^k}}\,\overline{\vec{V}_r^{M^k}} C_{M^k} + \sum_{i=1}^{m^k} \overline{\vec{S}_i} \tag{B14}$$

where C_{M^k-1} and C_{M^k} are the correlation functions between charges and the relative velocities of the fragments generated through the decay of the source labeled with M'^k. We now assume that $t > t_{\rm eq}$; $t_{\rm eq}$ is a time after which one can consider statistical excitation of the dipolar mode and particles emission according to the compound nucleus mechanism. Under this condition, we get

$$\overline{\vec{S}_i} = 0 \qquad i = 1, m^k, \tag{B15}$$

$$\overline{\vec{V}_r^{M^k-1}} = \overline{\vec{V}_r^{M^k}} = 0. \tag{B16}$$

The first equation reflects the definition itself of dipolar statistical excitations (see also Ref. [22]). In fact, in this case the dipolar signals correspond to the fluctuations around the ensemble averages. The ensemble averages of these signals are zero by definition. The second equation reflects the results of the isotropic emission that characterizes the particle decay from a hot compound nucleus. Therefore, we finally obtain

$$\overline{\vec{V}^k(t \to \infty)} = \overline{\vec{V}^k(t > t_{eq})}, \tag{B17}$$

which is just Eq. (10) of the text.

[1] J. O. Newton, B. Herskind, R. M. Diamond, E. L. Dines, J. E. Draper, K. H. Lindenberger, C. Schuck, S. Shih, and F. S. Stephens, Phys. Rev. Lett. **46**, 1383 (1981).
[2] K. A. Snover, Annu. Rev. Nucl. Part. Sci. **36**, 545 (1986).
[3] M. Thoennessen, D. R. Chakrabarty, M. G. Herman, R. Butsch, and P. Paul, Phys. Rev. Lett. **59**, 2860 (1987).
[4] J. J. Gaardhoje, A. M. Bruce, and B. Herskind, Nucl. Phys. **A482**, 121c (1988).
[5] D. Brink, Nucl. Phys. **A519**, 3c (1990).
[6] V. V. Kamanin, A. Kugler Yu, G. Sobolev, and A. S. Formicheu, Z. Phys. A **337**, 111 (1990).
[7] Y. Alhassid and B. Bush, Nucl. Phys. **A509**, 461 (1990).
[8] J. J. Gaardhoje, Annu. Rev. Nucl. Part. Sci. **42**, 483 (1992).
[9] L. Campaiola *et al*., Nucl. Phys. **A583**, 119 (1995).
[10] L. Campaiola *et al*., Z. Phys. A **352**, 421 (1995).
[11] S. Flibotte *et al*., Phys. Rev. Lett. **77**, 1448 (1996), and reference therein.
[12] T. Suomijarvi *et al*., Phys. Rev. C **53**, 2258 (1996).
[13] F. Amorini, M. Cabibbo, G. Cardella, A. Di Pietro, P. Figuera, A. Musumarra, M. Papa, G. Pappalardo, F. Rizzo, and S. Tudisco, Phys. Rev. C **58**, 987 (1998).
[14] M. Papa, F. Amorini, M. Cabibbo, G. Cardella, A. Di Pietro, P. Figuera, A. Musumarra, G. Pappalardo, F. Rizzo, and S. Tudisco, Eur. Phys. J. A **4**, 69 (1999).
[15] D. Kusnezov, Y. Alhassid, and K. A. Snover, Phys. Rev. Lett. **81**, 542 (1998).
[16] B. Bush and Y. Alhassid, Nucl. Phys. **A531**, 27 (1991).
[17] K. A. Snover, Nucl. Phys. **A687**, 337c (2001).
[18] N. P. Shaw *et al*., Phys. Rev. C **61**, 044612 (2000).
[19] S. K. Hui *et al*., Phys. Rev. C **62**, 054604 (2000).
[20] S. Tudisco *et al*., in *Proceedings of 'Experimental Nuclear Physics in Europe:ENPE99: Facing the next Millennium*, June 21–25, 1999, Sevilla (Spain), edited by B. Rubio *et al*. (AIP, Melville, NY) p. 323.
[21] S. Tudisco *et al*., Europhys. Lett. **58**, 811 (2001).
[22] M. Papa *et al*., Phys. Rev. C **68**, 034606 (2003).
[23] D. Pierroutsakou *et al*., Eur. Phys. J. A **16**, 423 (2003).
[24] D. Pierroutsakou *et al*., Eur. Phys. J. A **17**, 71 (2003).
[25] F. Amorini *et al*., Phys. Rev. C **69**, 014608 (2004).
[26] P. Heckman *et al*., Nucl. Phys. **A750**, 245 (2005).
[27] J. Seitz *et al*., Nucl. Phys. **A750**, 175 (2005).
[28] M. Papa, G. Giuliani, and A. Bonasera, J. Comput. Phys. **208**, 403 (2005).
[29] F. Puhlhofer, Nucl. Phys. **A280**, 267 (1977).
[30] M. Papa, T. Maruyama, and A. Bonasera, Phys. Rev. C **64**, 024612 (2001).
[31] A. Musumarra, G. Cardella, A. Di Pietro, S. L. Li, M. Papa, G. Pappalardo, F. Rizzo, and S. Tudisco, Nucl. Instrum. Methods A **370**, 558 (1996), and reference therein.

[32] A. D. Pietro *et al*., Nucl. Phys. **A689**, 668 (2001).
[33] A. Musumarra *et al*., Nucl. Instrum. Methods A **409**, 414 (1998).
[34] J. Lu, P. Figuera, F. Amorini, G. Cardella, A. Di Pietro, A. Musumarra, M. Papa, G. Pappalardo, F. Rizzo, and S. Tudisco, Nucl. Instrum. Methods A **471**, 374 (2001).
[35] G. Casini, P. R. Maurenzing, A. Olmi, and A. A. Stefanini, Nucl. Instrum. Methods A **277**, 445 (1989).
[36] R. J. Charity *et al*., Nucl. Phys. **A483**, 371 (1988).
[37] V. Baran, D. M. Brink, M. Colonna, and M. Di Toro, Phys. Rev. Lett. **87**, 182501 (2001).
[38] P. F. Bortignon, M. Braguti, D. M. Brink, R. A. Broglia, C. Brusati, F. Camera, W. Cassing, M. Cavinato, N. Giovanardi, and F. Gulminelli, Nucl. Phys. **A583**, 101c (1995).
[39] P. Chomaz, M. Di Toro, and A. Smerzi, Nucl. Phys. **A563**, 509 (1993).
[40] L. Shi and P. Danielewicz, Phys. Rev. C **68**, 064604 (2003).
[41] B. A. Li, Phys. Rev. C **69**, 034614 (2004).